SCIENCE CHINA
Chemistry

• ARTICLES •
• SPECIAL TOPIC • The Frontiers of Chemical Biology and Synthesis

January 2011 Vol.54 No.1: 137–143
doi: 10.1007/s11426-010-4177-7

# Self-assembly of anisotropic tobacco mosaic virus nanoparticles on gold substrate

PENG Bo[1], LIU NingNing[2], LIN Yuan[1,3], WANG LiMing[1], ZHANG WenKe[2], NIU ZhongWei[3†], WANG Qian[3*] & SU ZhaoHui[1*]

[1]*State Key Laboratory of Polymer Physics and Chemistry, Changchun Institute of Applied Chemistry, Chinese Academy of Sciences, Changchun 130022, China*
[2]*State Key Laboratory of Supramolecular Structure and Materials, College of Chemistry, Jilin University, Changchun 130012, China*
[3]*Department of Chemistry and Biochemistry and Nanocenter, University of South Carolina, Columbia, SC 29208, USA*

Received July 20, 2010; accepted September 24, 2010

A facile approach to assembled virus film with tunable structure is presented. Rod-like tobacco mosaic virus (TMV) was selected as the prototype in this study for its anisotropic structural feature. TMV can either "lie down" or "stand up" on gold substrate by tuning the solution pH. A quartz crystal microbalance with dissipation monitoring was used to monitor the pH-dependent self-assembly behavior of TMV nanoparticles, and atomic force microscopy and single molecule force spectroscopy further confirmed the different assembly structures.

**tobacco mosaic virus, self-assembly, quartz crystal microbalance with dissipation, single molecule force spectroscopy**

## 1 Introduction

A major objective in nanoscience and nanotechnology is to carry nano-objects from bulk to surfaces and to control the assembly structure [1]. Self-assembly of biological building blocks to form hierarchically ordered structures offers novel scaffolds for developing materials and devices at a nanoscale level [2–4]. Virus nanoparticles (VNPs) are distinctive in that they are made from regular biomolecular building units, and can self-assemble into sophisticated structures with well-defined morphologies and sizes [5, 6]. Moreover, the VNP's surface allows for the decoration of the particle with multiple functionalities [7].

Recently, the fabrication of multilayered biological thin films has drawn lots of attention due to their wide applications as cell culture substrates, biological sensors and reactors. By this technique, biomacromolecules can be assembled into thin films with controlled structure [7]. However, most of these studies focused on globular or irregular particles. In fact, assembling anisotropic nano-objects is interesting because the anisotropic shape of these particles can result in unique optical and electrical properties [8]. Furthermore, anisotropic rod-like particles may exhibit more interesting assembly behavior, the study of which will help understand the complex mechanism of protein assembly on solid/liquid interface.

Tobacco mosaic virus (TMV) is a well-characterized rod-like plant virus. It is a nanotube of 300 nm in length and 18 nm in diameter with a 4 nm-wide interior channel. The virus is composed of ~2130 identical coat protein subunits helically assembling and wrapping around a single RNA strand. TMV exhibits remarkable stability at temperatures up to 60 °C and in pH range from 2 to 10 [9], and thus is an excellent building block for constructing biological thin films. Recent research showed that surface modification of TMV could be achieved via chemical or genetic methods

*Corresponding author (email: wang@mail.chem.sc.edu; zhsu@ciac.jl.cn)
†Current address: Technical Institute of Physics and Chemistry, Chinese Academy of Sciences, Beijing 100190, China

without disrupting the integrity and morphology of the capsid [10–12], which can further expand the functionalities of TMV as a nano building block. The chemically modified and genetically engineered viruses have been used to direct the synthesis of materials by controlling composition, mutation positions and morphologies [13–20]. Since TMV is an anisotropic rod-like nanoparticle, it is important to control its alignment and orientation in the assemblies. For example, it has been reported that after coating cobalt on the outer surface, thin films composed of vertically aligned TMV nanoparticles can be used as battery electrodes [21]. To achieve the vertical alignment required for this application, a cysteine mutant TMV was needed [21].

Owing to its high sensitivity and its ability to provide information on both the mass of surface-bound molecules and the viscoelastic properties of adlayers in real time, quartz crystal microbalance with dissipation monitoring (QCM-D) has found increasing applications in the studies of intermolecular interactions between antibody and antigen [22] or between DNA and peptide [23], as well as the adsorption kinetics of cells on polymer surfaces [24]. This technique has also been applied to monitor the adsorption behavior of virus particles on polyelectrolyte films [6, 25]. In the present work, we use QCM-D to study the assembly behavior of TMV on gold substrate, and in conjunction with atomic force microscopy (AFM) imaging and single molecule force spectroscopy (SMFS) studies. The results show that by controlling solution pH, when adsorbed to gold substrate, native TMV can either align horizontally or vertically on the surface.

## 2 Experimental

### 2.1 Materials

Sodium dihydrogen phosphate dehydrate and disodium hydrogen phosphate dodecahydrate were purchased from Aldrich Co. (USA) and used without further purification; ammonia hydroxide (25%) and hydrogen peroxide (30%) were purchased from Beijing Chemical Plant (China) and used as received. Water was purified using a Millipore Milli-Q system (18.2 MΩ.cm). TMV particles were isolated from infected plants as previously described [26].

### 2.2 QCM-D measurements

The adsorption of the TMV was characterized with a quartz crystal microbalance with dissipation (QCM-D, Q-Sense E1, Sweden) equipped with a QFM 401 flow module. The sensor was an AT-cut piezoelectric quartz crystal (cut at 35° to the *y*-axis) sandwiched between two gold electrodes, and for all measurements QSX 301 Gold sensors were used. The constant ($C$) of the crystal was 17.7 ng/cm$^2$/Hz. Because the crystals were polished with an rms roughness of less than 3 nm, the effects of surface roughness were neglected [27]. A gold-coated chip (the sensor) was first cleaned by immersion in a 2% SDS solution for 30 min, rinsing with Milli-Q water, and blow-drying with a stream of nitrogen. The sensor was then heated in an ammonium peroxide mixture (5:1:1 mixture of Milli-Q water, ammonia (25%) and hydrogen peroxide (30%)) to 75 °C, rinsed with Milli-Q water and dried with a stream of nitrogen. (Caution: The ammonium peroxide mix solution should be used in a fume hood, with proper protection (eyewear and gloves)). After this treatment, the freshly cleaned chip was mounted in a QFM 401 chamber (Q-Sense, Gothenburg, Sweden) with one side exposed to the solution [28]. Before and after each introduction of TMV (0.5 mg/mL in 0.1 M potassium phosphate buffer) into the system the chip was exposed to a buffer of the same pH.

Briefly, when the surface of a sensor crystal adsorbs (soft) matter, changes in its resonance frequency ($\Delta f$) related to the mass attached (including coupled water), and in its dissipation ($\Delta D$) related to frictional (viscous) losses in the adlayer, are measured with a time resolution of better than 1 s. In air or vacuum, if the added layer is rigid, and much thinner than the crystal, the frequency shift ($\Delta f$) is related to mass loaded ($\Delta m$) and the overtone number ($n = 1, 3, 5, ...$) by the Sauerbrey equation [29],

$$\Delta m = -\frac{\rho_q l_q}{f_0}\frac{\Delta f}{n}$$

where $f_0$ is the fundamental frequency, and $l_q$ and $\rho_q$ are the thickness and density of the quartz crystal, respectively. The dissipation factor is given by [30]

$$\Delta D = \frac{E_{\text{dissipated}}}{2\pi E_{\text{stored}}}$$

where $E_{\text{dissipated}}$ and $E_{\text{stored}}$ are the energy dissipated during one period of oscillation and the energy stored in the oscillating system, respectively. The measurement of $\Delta D$ is based on the fact that the voltage over the crystal decays exponentially as a damped sinusoidal when the driving power of a piezoelectric oscillator is switched off [30]. By switching the driving voltage on and off periodically, a series of changes in the resonant frequency and the dissipation factor are obtained.

### 2.3 Atomic force microscopy imaging

AFM imaging experiments were performed on a commercial scanning probe microscope (SPA300HV, with a SPI3800N Probe Station, Seiko Instruments Inc., Japan). Tapping mode was used to study the surface structure. Silicon tips with a frequency of 63–70 kHz and a spring constant of 2 N/m were used. To prepare the specimen for AFM imaging, a freshly cleaned gold chip was immersed in the virus solution for 100 min, and then removed from the solution, washed with Milli-Q water and dried in ambient.

### 2.4 Single molecule force spectroscopy

SMFS experiments were carried out using a NanoWizard II BioAFM (JPK instrument AG, Berlin, Germany) in contact mode at room temperature. The TMVs were detected using untreated $Si_3N_4$ AFM tips (Veeco, CA). The spring constant of the AFM cantilevers employed were calibrated using the thermal noise method [31, 32]. The measured values ranged from 20 to 25 pN/nm.

### 2.5 Transmission electron microscopy

TEM observations were carried out on a JEOL 1011 microscope operating at 100 kV. The camera length was calibrated with Au standard. The virus was dissolved in water and the solution pH was tuned using hydrochloric acid (HCl) and sodium hydroxide (NaOH).

## 3 Results and discussion

QCM-D is a powerful tool for adsorption study. It monitors resonance frequency shift ($\Delta f$) and changes in dissipation ($\Delta D$) in real time when adsorption occurs on the surface of its sensor, which typically is a Au-coated quartz crystal. The resonance frequency ($f$) and the dissipation ($D$) of the quartz crystal are determined as described by Rodahl *et al*. [33]. The dissipation ($\Delta D$) is measured by switching off the driving voltage and monitoring the amplitude decay, which gives the information about the viscoelastic properties of the film. The more viscoelastic is the film, the higher is the energy loss (dissipation) and hence $\Delta D$. A small mass added to the sensor ($\Delta m$) induces a decrease in the resonance frequency ($\Delta f$), which is proportional to $\Delta m$, provided that the mass is small compared to the weight of the crystal and is evenly distributed, does not slip or deform on the electrode, and is sufficiently rigid or thin to have negligible internal friction (i.e. $\Delta D$ is small). In this case Sauerbrey equation [34] applies:

$$\Delta m = -\frac{C\Delta f}{n}$$

where $C$ ($C = 17.7$ ng/cm$^2$/Hz at $f = 5$ MHz) is the mass-sensitivity constant and $n$ ($n = 1, 3, 5, ...$) is the overtone number. If $\Delta D$ is high, the Sauerbrey equation is no longer valid, and the data can be analyzed by fitting to a viscoelastic Voigt model [35], in which the density, thickness and elastic shear modulus of the adsorbed layer are taken into account.

Figure 1 shows the $\Delta f$ and $\Delta D$ as functions of time for TMV adsorption onto gold substrate at different pH. The

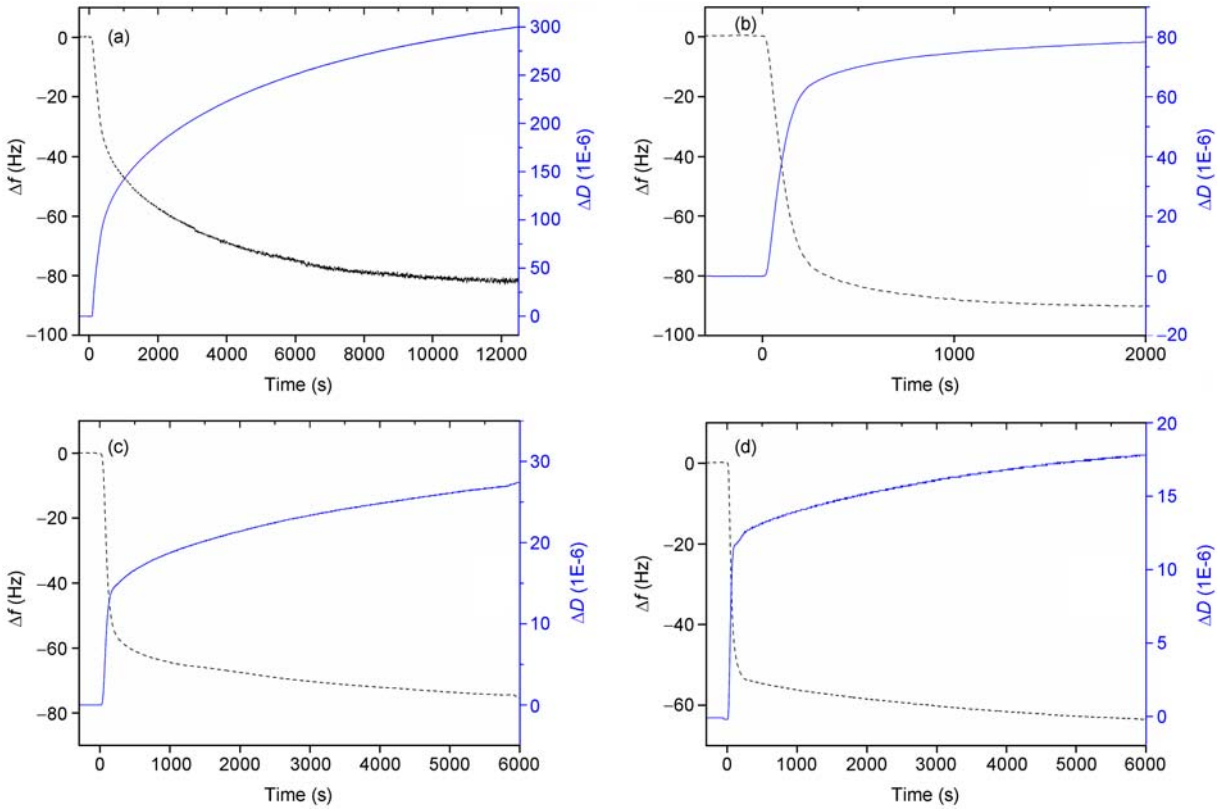


**Figure 1** QCM-D measurement of TMV adsorption on gold, showing $\Delta f$ (black dash line) and $\Delta D$ (blue solid line) vs. time at pH of (a) 4.7, (b) 6.9, (c) 7.4, and (d) 8.0.

decrease of $\Delta f$ equates to an increase in $\Delta m$, and consequently indicates that virus particles have self-assembled on the gold-coated sensor surface. In all cases the $\Delta f$ first decreases quickly in the early stage, and then slowly approaches a steady state over a much longer period of time. The $\Delta D$ plot is almost the mirror image of the $\Delta f$ curve, exhibiting the same two-stage pattern in all four cases. These patterns suggest that the TMV assembly involves two distinct steps: in the very beginning TMVs adsorb to the surface rapidly and in large quantity, occupying most of the adsorption sites on the substrate surface, and then TMV particles continue to attach to the surface in a much slower rate, while the adsorbed TMVs may rearrange their configuration and packing at the same time until the surface is saturated. Although the transition between the two stages is not well defined at pH 4.7, it can be better identified for the other three cases.

It is clear that changing the pH from acidic to neutral and slightly basic has strong effects on the TMV adsorption kinetics. For the first stage of the adsorption, the higher the pH, the steeper the $\Delta f$ curve, and at pH 4.7, the adsorption reaches saturation at ~3 h, while at pH 6.9, the amount of adsorption levels off after ~0.5 h. That is, the kinetics is much faster at higher pH in both stages of the TMV adsorption. Furthermore, at the adsorption saturation time, the $\Delta f$ observed at different pHs are similar, in the range of 60–90 Hz, which indicates that similar amounts of mass (TMVs coupled with water) are assembled onto the gold substrate, but the $\Delta D$ values are quite different. At pH 4.7, the $\Delta D$ is around 300, suggesting a thicker and more loosely-packed structure, and it decreases with the increase of the pH. At pH 8.0, the $\Delta D$ is only 18, indicative of a more rigid adlayer. These results indicate that the binding mode of the virus particles is more complex at lower pH than that higher ones.

On the other hand, it can be seen from Figures 1(c) and (d) that at pH 7.4 and 8.0, the pH does not affect the $\Delta f$ and $\Delta D$ markedly. This is consistent with the results of Brenner and Mcquarrie [36]. At these pH, much higher than the isoelectric point (pI) of TMV (~3.4), the TMV particles carry large amount of negative charges. As reported by Fraden and Purdy *et al*. previously, for a highly charged particle such as TMV (~20 $e^-$/nm), the effective diameter of TMV is insensitive to the variation of surface charge density induced by the changes of pH in aqueous solution in this regime (pH>7) [37, 38].

One may expect that rod-like particles can bind to gold substrate in various conformations and form different assembly structures, such as flat, angled, or vertical with respect to the substrate surface. In order to make a clear sense, all overtones of the $\Delta f$ and $\Delta D$ data were further modeled according to the Voigt model by using QTools software [35] to estimate the thickness of the virus layer. The results are summarized in Table 1.

At pH 7.4 and 8.0, the mass of the adsorbed layer is slightly lower than the value for a close-packed TMV layer. The fitted layer thickness is around 50 nm, greater than the diameter of TMV, which is 18 nm, but much smaller than the length of TMV, which is 300 nm. These numbers suggest that at higher pH, the rod-like TMV particles tend to lay down on the gold substrate, and some may lie across over one another, forming a thin and more rigid layer, whereas at lower pH, the TMVs tend to stand up on one end, forming a thick and loose layer.

**Table 1** Frequency shift, dissipation change, and layer thickness at different pH of the virus solution

| pH | $\Delta f$ (Hz) | $\Delta D$ (1E-6) | Thickness [a] (nm) |
|---|---|---|---|
| 4.7 | 80 | 300 | 260 |
| 6.9 | 90 | 77 | 111 |
| 7.4 | 74 | 26 | 50 |
| 8.0 | 63 | 18 | 49 |

a) Thickness of the virus layers was modelled according to the Voigt model by using QTools software. All overtones (3, 5, 7, 9…) have been used.

The above results obtained by QCM-D provide an overall assessment of the TMV layer assembled, and it is necessary to investigate the structure of assembly in more detail in order to better understand the assembly behavior of TMV. Figure 2 shows the TEM images of TMV assembly obtained at two different pH. It can be seen that at pH 4.8, the TMV nanotubes tend to aggregate into bundles, whereas at pH 7.2, they are well dispersed as individual nanotubes. This can be attributed to the surface charges carried by the TMV. Since the pI of TMV is around 3.4, at pH 4.8, near the pI, the net charge on the TMV surface is low, resulting in small electrostatic repulsion forces between the TMVs, and lots of the less negatively charged nanotubes are easily bound together due to weak interactions (van der Waals and hydrophobic interactions). On the other hand, at pH 7.2, far away from the pI, TMV carries much more negative charges on its surface. Due to the high negative charge density on the surface, the electrostatic repulsions among TMV particles increase [39–42]. As a result, TMVs are repulsive to each other and are randomly dispersed on the TEM grid (Figure 2(b)).

The virus assembly on gold substrate was then character-

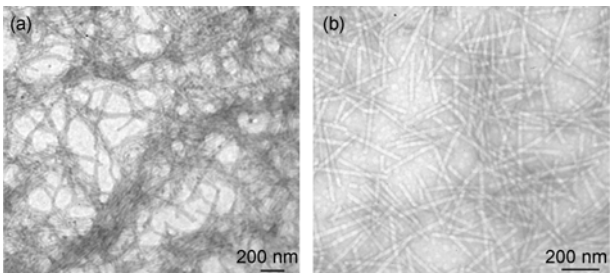


**Figure 2** TEM images of TMV at pH 4.8 (a) and pH 7.2 (b).

ized using AFM-based single molecule force spectroscopy (SMFS) [43]. The SMFS experimental details have been described elsewhere [44]. Briefly, TMV particles are immobilized on a freshly cleaned gold substrate by physical adsorption, and as shown in Figure 3. AFM tip is then brought to contact with the TMV sample layer. The sample is stationary, whereas the AFM tip moves along $z$-axis controlled by a piezo tube. When the AFM tip approaches the sample surface and contacts a TMV particle, a repulsive force between them is detected by the deflection of the AFM cantilever (position B). Further movements of the AFM tip toward the gold substrate surface causes the bending or breaking of the TMV particle, and the rod-like particle either snaps or slides off the AFM tip, causing a sudden drop in the force detected (position C). The AFM tip finally touches the solid substrate, producing a repulsion signal at close to height zero (position D). Then the tip is moved away from the sample surface and back to its original position (position A). A scan cycle is thus complete and a force-vs-distance profile including an approach curve (A–D, in black) and a retraction curve (D–A, in red) is obtained. The apparent height of the TMV particle relative to the gold surface can be determined by measuring the lateral distance between position B and D in the approach curve.

Figure 4 presents the height distribution of TMV assembled on gold substrates at different pH measured by the afore-mentioned AFM-based SMFS. Most of the heights of the virus particles are in the range of 20–70 nm for the layer assembled at pH 7.4. However, at pH 4.7, the heights of the viruses are in the range of 270–300 nm. Since the SMFS measurements give the apparent hight of individual TMV partciles instead of the layer thickness, we can tell the orientation of TMV particles relative to the gold surface using based on the height results. If it is a multilayered

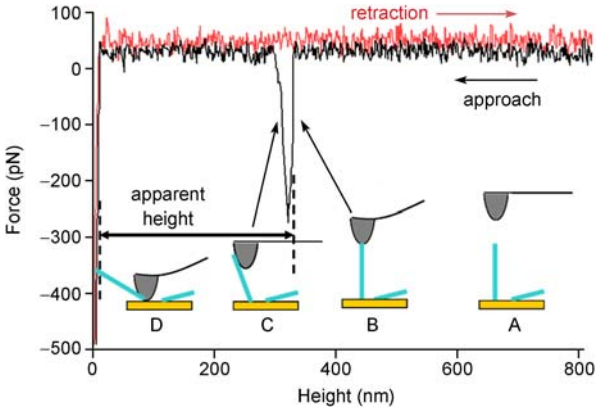


**Figure 3** Approach and retraction curves during a complete force scan, and the experimental principle for determining the apparent height of a TMV particle immobilized on the gold surface. At position A, the AFM tip is far away from the sample; AFM tip touches a TMV particle at position B; the TMV particle either becomes broken or slides off the AFM tip at position C; the tip finally touches the solid substrate at position D.

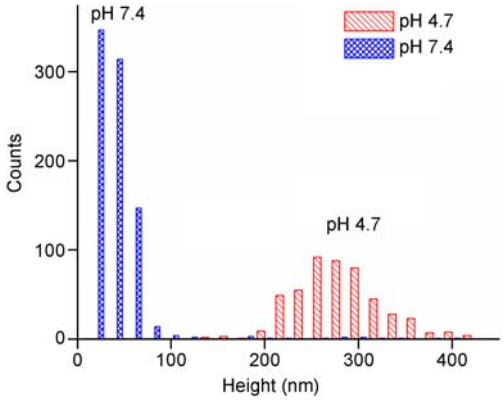


**Figure 4** AFM-based SMFS height distribution of TMVs assembled at pH 7.4, and 4.7.

TMV assembled at pH 4.7, the SMFS and AFM images of the top layer should be similar to that of pH 7.4. In addition, the data from directly measurements are in good agreement with the QCM-D model-fitting results discussed above, and again confirm that TMV has different assembly behavior on gold surface depending on pH of the solution.

The packing of TMV particles on gold surface was also directly assessed by AFM imaging operated in tapping mode, and the morphologies of the TMV assembly are shown in Figure 5. For the layer assembled at pH 7.4, rod-like TMVs are clearly seen lying all over the gold surface (Figure 5(b)), whereas for the film fabricated at pH 4.7, few rod-like objects can be identified in the AFM image (Figure 5(a)). Most of TMV particles appear to stand on one end on the gold surface and aggregate into vertical bundles, similar to that observed for cysteine mutant TMVs [21]. That is the reason why the heights detected by SMFS were in the range of 270–300 nm, and high $\Delta D$ as well as low $\Delta f$ values were obtained by QCM-D at pH 4.7, and at pH 7.4 the height of the film fell in the range of 20–70 nm. Based on all the above experimental results and analyses, the possible configurations of TMVs assembled on gold surface are schematically illustrated in Figure 6.

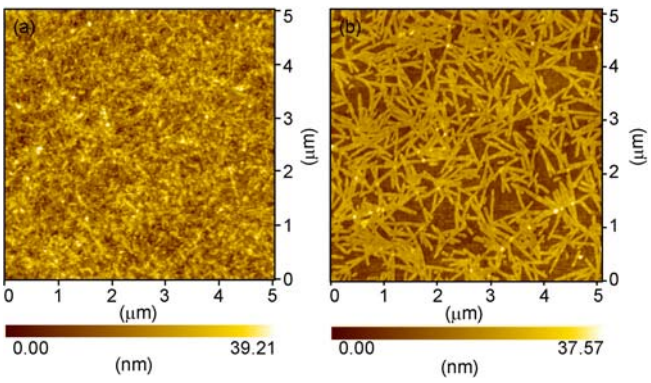


**Figure 5** AFM height images of the TMV layer on the gold surface assembled at pH 4.7 (a) and 7.4 (b), respectively.

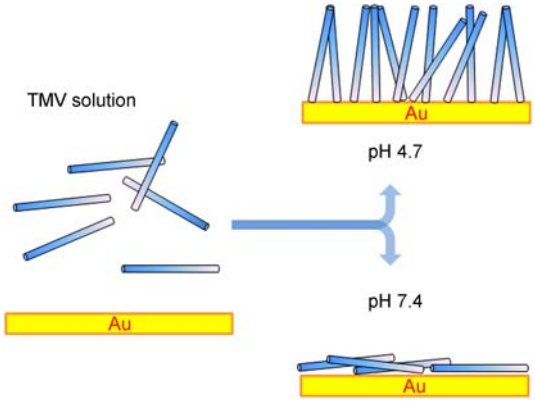


**Figure 6** Schematic illustration of TMVs assembled on the gold surface at different pHs.

## 4 Conclusions

We have studied the assembly of rod-like TMV particles on gold substrate, and demonstrated that pH has strong effects on the kinetics and the structure of TMV assemblies. At low pH (close to the pI of TMV), the TMV particle carries less negative charges on its surface, so that the assembly of TMVs on the gold substrate is relatively slow, and the particles tend to attach to the substrate on one end and stand vertically on the surface, resulting in a thick and loose layer. At high pH (pH > pI), much more negative charges are present on the TMV surface, and the stronger interactions between the viral particles and the surface lead to much faster adsorption kinetics, and the rod-like particles tend to lie down on the substrate surface, forming a much thinner and more rigid assembly layer. This work helps the understanding of the complex assembly behavior of anisotropic nanoparticles, and affords a facile way for tuning the assembly structure of viral nanoparticles for potential applications in electronics, optics, sensing, and biomedical engineering.

*This work was supported by the National Natural Science Foundation of China (20423003 & 20774097). Z.S. thanks the NSFC Fund for Creative Research Groups (50921062) for support. Q.W. thanks the financial support from US NSF (DMR-0706431, CHE-0748690), US DoD, US DoE-BES, and the W. M. Keck Foundation.*

1 Hammond PT. Form and function in multilayer assembly: New applications at the nanoscale. *Adv Mater*, 2004, 16: 1271–1293
2 Horn A, Schoberth HG, Hiltl S, Chiche A, Wang Q, Schweikart A, Fery A, Boker A. Nanostructured wrinkled surfaces for templating bionanoparticles-controlling and quantifying the degree of order. *Farad Discuss*, 2009, 143: 143–150
3 Manocchi AK, Seifert S, Lee B, Yi H. On the thermal stability of surface-assembled viral-metal nanoparticle complexes. *Langmuir*, 2010, 26: 7516–7522
4 Yi H, Rubloff GW, Culver JN. TMV microarrays: Hybridization-based assembly of DNA-programmed viral nanotemplates. *Langmuir*, 2007, 23: 2663–2667
5 Kaur G, He JB, Xu J, Pingali SV, Jutz G, Boker A, Niu ZW, Li T, Rawlinson D, Emrick T, Lee B, Thiyagarajan P, Russell TP, Wang Q. Interfacial assembly of turnip yellow mosaic virus nanoparticles. *Langmuir*, 2009, 25: 5168–5176
6 Steinmetz NF, Bock E, Richter RP, Spatz JP, Lomonossoff GP, Evans DJ. Assembly of multilayer arrays of viral nanoparticles via biospecific recognition: A quartz crystal microbalance with dissipation monitoring study. *Biomacromolecules*, 2008, 9: 456–462
7 He JB, Niu ZW, Tangirala R, Wang JY, Wei X, Kaur G, Wang Q, Jutz G, Böker A, Lee B, Pingali SV, Thiyagarajan P, Emrick T, Russell TP. Self-assembly of tobacco mosaic virus at oil/water interfaces. *Langmuir*, 2009, 25: 4979–4987
8 Bittner AM. Biomolecular rods and tubes in nanotechnology. *Naturwissenschaften*, 2005, 92: 51–64
9 Shenton W, Douglas T, Young M, Stubbs G, Mann S. Inorganic-organic nanotube composites from template mineralization of tobacco mosaic virus. *Adv Mater*, 1999, 11: 253–256
10 Bruckman MA, Kaur G, Lee LA, Xie F, Sepulvecla J, Breitenkamp R, Zhang X, Joralemon M, Russell TP, Emrick T, Wang Q. Surface modification of tobacco mosaic virus with "click" chemistry. *Chembiochem*, 2008, 9: 519–523
11 Schlick TL, Ding ZB, Kovacs EW, Francis MB. Dual-surface modification of the tobacco mosaic virus. *J Am Chem Soc*, 2005, 127: 3718–3723
12 Yi H, Nisar S, Lee S-Y, Powers MA, Bentley WE, Payne GF, Ghodssi R, Rubloff GW, Harris MT Culver JN. Patterned assembly of genetically modified viral nanotemplates via nucleic acid hybridization. *Nano Lett*, 2005, 5: 1931–1936
13 Douglas T, Young M. Host-guest encapsulation of materials by assembled virus protein cages. *Nature*, 1998, 393: 152–155
14 Douglas T, Young M. Viruses: Making friends with old foes. *Science*, 2006, 312: 873–875
15 Lee SW, Mao CB, Flynn CE, Belcher AM. Ordering of quantum dots using genetically engineered viruses. *Science*, 2002, 296: 892–895
16 Mao CB, Solis DJ, Reiss BD, Kottmann ST, Sweeney RY, Hayhurst A, Georgiou G, Iverson B, Belcher AM. Virus-based toolkit for the directed synthesis of magnetic and semiconducting nanowires. *Science*, 2004, 303: 213–217
17 Miller RA, Presley AD, Francis MB. Self-assembling light-harvesting systems from synthetically modified tobacco mosaic virus coat proteins. *J Am Chem Soc*, 2007, 129: 3104–3109
18 Nam KT, Kim DW, Yoo PJ, Chiang CY, Meethong N, Hammond PT, Chiang YM, Belcher AM. Virus-enabled synthesis and assembly of nanowires for lithium ion battery electrodes. *Science*, 2006, 312: 885–888
19 Niu ZW, Liu J, Lee LA, Bruckman MA, Zhao DG, Koley G, Wang Q. Biological templated synthesis of water-soluble conductive polymeric nanowires. *Nano Lett*, 2007, 7: 3729–3733
20 Wang Q, Lin TW, Tang L, Johnson JE, Finn MG. Icosahedral virus particles as addressable nanoscale building blocks. *Angew Chem Int Ed*, 2002, 41: 459–462
21 Royston E, Ghosh A, Kofinas P, Harris MT, Culver JN. Self-assembly of virus-structured high surface area nanomaterials and their application as battery electrodes. *Langmuir*, 2008, 24: 906–912
22 Hook F, Voros J, Rodahl M, Kurrat R, Boni P, Ramsden JJ, Textor M, Spencer ND, Tengvall P, Gold J, Kasemo B. A comparative study of protein adsorption on titanium oxide surfaces using in situ ellipsometry, optical waveguide lightmode spectroscopy, and quartz crystal microbalance/dissipation. *Colloid Surf B-Biointerf*, 2002, 24: 155–170
23 Hook F, Ray A, Norden B, Kasemo B. Characterization of PNA and DNA immobilization and subsequent hybridization with DNA using acoustic-shear-wave attenuation measurements. *Langmuir*, 2001, 17: 8305–8312
24 Svedhem S, Dahlborg D, Ekeroth J, Kelly J, Hook F, Gold J. *In situ* peptide-modified supported lipid bilayers for controlled cell attachment. *Langmuir*, 2003, 19: 6730–6736
25 Steinmetz NF, Findlay KC, Noel TR, Parker R, Lomonossoff GR, Evans DJ. Layer-by-layer assembly of viral nanoparticles and polyelectrolytes: The film architecture is different for spheres versus rods. *Chembiochem*, 2008, 9: 1662–1670
26 Niu ZW, Bruckman MA, Li SQ, Lee LA, Lee B, Pingali SV, Thiya-

garajan P, Wang Q. Assembly of tobacco mosaic virus into fibrous and macroscopic bundled arrays mediated by surface aniline polymerization. *Langmuir*, 2007, 23: 6719–6724
27 Martin SJ, Frye GC, Ricco AJ, Senturia SD. Effect of surface roughness on the response of thickness-shear mode resonators in liquids. *Anal Chem.* 1993, 65: 2910–2922
28 Kern W, Puotinen DA. Cleaning solutions based on hydrogen peroxide for use in silicon semiconductor technology. *RCA Review*, 1970, 31: 187–206
29 Liu GM, Zhang GZ. Periodic swelling and collapse of polyelectrolyte brushes driven by chemical oscillation. *J Phys Chem B*, 2008, 112: 10137–10141
30 Rodahl M, Hook F, Krozer A, Brzezinski P, Kasemo B. Quartz-crystal microbalance setup for frequency and q-factor measurements in gaseous and liquid environments. *Rev Sci Instrum*, 1995, 66: 3924–3930
31 Butt HJ, Jaschke M. Calculation of thermal noise in atomic-force microscopy. *Nanotechnology*, 1995, 6: 1–7
32 Hutter JL, Bechhoefer J. Calibration of atomic-force microscope tips. *Rev Sci Instrum*, 1993, 64: 1868–1873
33 Olanya G, Iruthayaraj J, Poptoshev E, Makuska R, Vareikis A, Claesson PM. Adsorption characteristics of bottle-brush polymers on silica: Effect of side chain and charge density. *Langmuir*, 2008, 24: 5341–5349
34 Sauerbrey G. Verwendung von Schwingquarzen zur Wägung dünner Schichten und zur Mikrowägung. *Zeitschrift für Physik A Hadrons Nuclei*, 1959, 155: 206–222
35 Voinova MV, Rodahl M, Jonson M, Kasemo B. Viscoelastic acoustic response of layered polymer films at fluid-solid interfaces: Continuum mechanics approach. *Phys Scr*, 1999, 59: 391–396
36 Brenner SL, McQuarrie DA. On the theory of the electrostatic interaction between parallel cylindrical polyelectrolytes. *J Colloid Interface Sci.* 1973, 44: 298–317
37 Fraden S, Maret G, Caspar DLD. Angular correlations and the isotropic-nematic phase-transition in suspensions of tobacco mosaic-virus. *Phys Rev E*, 1993, 48: 2816–2837
38 Purdy KR, Fraden S. Isotropic-cholesteric phase transition of filamentous virus suspensions as a function of rod length and charge. *Phys Rev E*, 2004, 70: 061703
39 Martín-Rodríguez A, Cabrerizo-Vílchez MA, Hidalgo-Alvarez R. A comparative study on the electrokinetic behavior of bovine serum albumin molecules adsorbed onto different polymer colloids. *Colloid Surf A*, 1994, 92: 113–119
40 Peula JM, de las Nieves FJ. Adsorption of monomeric bovine serum albumin on sulfonated polystyrene model colloids 3. Colloidal stability of latex-protein complexes. *Colloid Surf A*, 1994, 90: 55–62
41 Peula JM, Puig J, Serra J, de las Nieves FJ, Hidalgo-Alvarez R. Electrokinetic characterization and colloidal stability of polystyrene latex particles partially covered by IgG/a-CRP and m-BSA proteins. *Colloid Surf A*, 1994, 92: 127–136
42 Wadu-Mesthrige K, Pati B, McClain WM, Liu GY. Disaggregation of tobacco mosaic virus by bovine serum albumin. *Langmuir*, 1996, 12: 3511–3515
43 Liu NN, Peng B, Lin Y, Su ZH, Niu ZW, Wang Q, Zhang WK, Li HB, Shen JC. Pulling genetic RNA of TMV using single molecula force spectroscopy. *J Am Chem Soc*, 2010, 132: 11036–11038
44 Zhang WK, Zhang X. Single molecule mechanochemistry of macromolecules. *Prog Polym Sci*, 2003, 28: 1271–1295